Article

Use of Sulfur Waste in the Production of Metakaolin-Based Geopolymers

Mazen Alshaaer [1,2,*], Abdulaziz O. S. Alanazi [1] and Ibrahim M. I. Absa [3]

1   Department of Physics, College of Science and Humanities in Al-Kharj, Prince Sattam bin Abdulaziz University, Al-Kharj 11942, Saudi Arabia; abdulazizaoda@gmail.com
2   Department Mechanics of Materials and Constructions, Vrije Universiteit Brussels (VUB), Pleinlaan 2, 1050 Brussels, Belgium
3   Hazardous and Solid Waste Department, Environment Quality Authority, Ramallah P606, Palestine; ibrahima@environment.pna.ps
*   Correspondence: mazen.alshaaer@vub.be

Abstract: This preliminary study introduces the incorporation and chemical stabilization of sulfur waste into a geopolymer matrix and explores the concept of material production for further environmental and engineering solutions. In this study, a novel synthesis procedure for sulfur-based geopolymers was introduced, and the role of sulfur in geopolymers and its optimal content to obtain a stable structure were explored. Geopolymers were synthesized by dissolving sulfur in an alkaline activator in different proportions. The alkaline solution was then mixed with metakaolin to synthesize the geopolymer matrix. Adding sulfur in amounts from 0 wt.% to 5 wt.%, compared with metakaolin, led to an increase in the compressive strength of the geopolymers from 22.5 MPa to 29.9 MPa. When sulfur was between 5 wt.% and 15 wt.%, a decrease in the compressive strength was observed to 15.7 MPa, which can be explained by defects and voids in the geopolymer's microstructure due to the solubility of excess sulfur. Because of the incorporation of sulfur into the geopolymers, a compact and dense microstructure was formed, as reported in the SEM analysis. An XRD analysis showed that, besides quartz and analcime, a new phase, $A_{l2} \cdot H_{10} \cdot O_{17} \cdot S_3$, was also formed as a result of sulfur dissolution in the alkaline activator of the geopolymers.

Keywords: sulfur; geopolymers; metakaolin; XRD

1. Introduction

Sulfur is a by-product of waste from gas production and oil facilities. The prediction of global sulfur production (according to United States Geological Survey (USGS) documents [1]) makes it important to seriously consider various alternative uses of sulfur, as well as its complete utilization (disposal) [2]. Based on the data for 2018, the total global production of sulfur was around 80 tons [3]. China is the main contributor of sulfur as a by-product, due to an increase in the number of gas-processing and refinery plants. The overall sulfur production in China is around 17 million tons [3]. The USA is the second-largest producer of sulfur, with a production capacity of around 9.7 million tons, followed by Russia, Saudi Arabia, and Canada with amounts of 7.1 million tons, 6 million tons, and 5.5 million tons, respectively. In addition, Japan and Kazakhstan each produce 3.5 million tons [3].

Sulfur is primarily produced as a by-product, so this is a unique industry compared to other mineral industries, which consume deposits and natural mineral resources. In addition, the demand and supply for sulfur are not stable and are unbalanced. For example, in the past decade, the production of sulfur has been much greater than the demand for this product, which was not the case a few decades ago. Globally, sulfur is almost exclusively an involuntary by-product of crude oil and sour gas processing to decrease sulfur dioxide emissions from the combustion of fossil-based energy sources [4]. One of the most common

compounds of sulfur is hydrogen sulfide (H_2S). Toxic hydrogen sulfide, among several sulfuric-based compounds, exists in sour gas. These compounds are removed by a stripping process, with the subsequent transformation of hydrogen sulfide to elemental sulfur. In addition, there are many organic sulfur species in crude oil, and their abundance varies from 1% to 3%. As a result of burning these organic sulfur species, anthropogenic sulfur emissions contribute to serious pollution problems such as acid rain, air pollution, and smog. Furthermore, the planetary albedo and cloud cover increase because of sulfate aerosols [5]. In the troposphere, this plays a role in climate cooling, thus slowing down the global warming phenomenon [6]. This has even led to propositions of using sulfuric acid/SO_2 for geoengineering, to mitigate climate change.

Geopolymers or alkali-activated materials [7–10] are prepared through the alkali activation of aluminum silicate precursors, where these aluminum silicates are transformed through geopolymerization reactions into stable and hard products of a tectosilicate nature [11]. Geopolymers have attractive and unique characteristics, such as the ability to harden at low temperatures or even in ambient conditions, excellent mechanical properties, and the possibility of green processing due to low gas emissions and a low energy consumption. They can be used in many important applications. Geopolymer-based materials are used in waste recycling and circular economies [12], the stabilization of toxic elements, water purification [13], and passive cooling systems [14]. However, geopolymer precursors and their processing are more costly than ordinary cement. One of the main components of geopolymers is an alkaline solution, which results in certain difficulties in field applications. To overcome these challenges, researchers have worked to develop novel strategies for the preparation of multi-functional and green geopolymer-based materials that can be used for different applications at the same time, such as construction and water purification purposes [15,16].

Geopolymers, as inorganic polymers, have unique and attractive characteristics, and have been extensively investigated for the stabilization/solidification of hazardous metallic and organic pollutants. The mechanism and efficiency of the stabilization and immobilization of metal ions such as Cu (II), Cd (II), Pb (II), and Cr (III) in the geopolymer matrix have been studied [17], and the results showed that these metals could be effectively stabilized and immobilized by geopolymerization. Several studies [18–20] have reported that solid waste, such as coal fly ash and slags, can be used as precursors or raw materials in geopolymer technology, concluding that these industrial wastes can be safely stabilized and capsulated through geopolymer transformation, or can be used for the stabilization/solidification of other hazardous waste. Therefore, geopolymer technology is characterized by its unique advantages for the stabilization and immobilization of hazardous pollutants [11]. The immobilization process for these ions is mainly based on the mechanisms of physical encapsulation, precipitation, sorption, and chemical bonding with lattice charges. In addition, geopolymers or alkali-activated materials have also been used for the stabilization/solidification of anionic pollutants, such as As oxyanions, Se oxyanions, and Cr oxyanions [21]. It has been confirmed that As and Se oxyanions can be associated in the geopolymer matrix through electrostatic interactions, despite the fact that the leaching of these elements is still higher compared to cationic metals.

Low-cost sulfur is available as a by-product in huge amounts, and it is a good candidate for reducing the costs of geopolymers and improving certain properties. Unfortunately, its solubility in water limits its use in geopolymer technology. Therefore, this study aims to develop a new methodology for processing sulfur-based geopolymers with a stable structure in the presence of water. The optimal content and the role of sulfur as a precursor or filler in geopolymers were investigated. The significance of this research is that it investigates methods for improving the properties of geopolymers and reducing their production costs, and it explores new applications for both sulfur and geopolymers.

2. Materials and Methods

2.1. Materials

Geopolymer cement was synthesized by using kaolinitic soil, a NaOH solution, and a Na_2SiO_3 solution. The kaolinitic soil sample was collected from a deposit in the Riyadh region (Saudi Arabia) with the assistance of the Saudi Ceramic Company. The chemical composition of the kaolinitic soil is shown in Table 1. The estimated kaolinite mass percentage in the precursor was 92% [14]. The kaolinitic soil was heated in a furnace (Nabertherm, USA) at 750 °C for 4 h to obtain amorphous kaolin (i.e., metakaolin).

Table 1. Chemical analysis of kaolinite.

Compound	Composition %
MnO	0.34
Cr_2O_3	0.45
CaO	1.11
K_2O	0.12
P_2O_5	0.93
Fe_2O_3	9.37
Al_2O_3	22.56
SiO_2	38.41
TiO_2	14.22

For the geopolymerization, alkali activator (Na_2SiO_3 and NaOH) solutions, which dissolve aluminosilicates, were prepared. The solution of sodium hydroxide (NaOH) was prepared by using pure pellets of sodium hydroxide (Merck, Germany) and deionized water. The Na_2SiO_3 solution consisted of 27 wt. % SiO_2 and 8 wt. % Na_2O [22–24].

The sulfur sample was prepared as a by-product from operations that included petroleum refining, heavy oil processing, and natural gas processing. The purity of the sample was around 99.9%. It was collected from the National Company for Sulphur Products (Riyadh, Saudi Arabia).

2.2. Preparation of Geopolymers

The alkali solutions of sodium hydroxide (NaOH) and sodium silicate (Na_2SiO_3) were mixed using Si/Na/Al with a molar ratio of ~1.5/1/1 [24]. The source of SiO_2 was the sodium silicate (Na_2SiO_3) solution and metakaolin ($Al_2O_3 \cdot 2SiO_2$), sodium oxide (Na_2O) resulted from the alkali activator solutions, and aluminum oxide (Al_2O_3) was obtained from the metakaolin ($Al_2O_3 \cdot 2SiO_2$). The molar ratio of H_2O/Na_2O in the alkaline solution was 6.3/1. To prepare the aqueous alkali solution, NaOH, H_2O, and Na_2SiO_3 were initially stirred for 5 min. The sulfur was ground to a size below 425 μm and was then dissolved into the alkaline solution by magnetic stirring for 6 h. The metakaolin was added to the sulfur–alkali solution, and then the solution was mechanically mixed for 10 min. Lastly, the resultant geopolymer mixture was cast into silicon molds of 20 mm × 20 mm × 40 mm, sealed, and left in an oven (Raypa, Spain) at 40 °C for 1 d to cure [14]. Afterward, the specimens were demolded and immersed for 3 d to evaluate their overall stability in the presence of water. Finally, the specimens were subjected to different characterization techniques. The descriptions and compositions of the geopolymer series are shown in Table 2 and Figure 1.

Table 2. Composition of the synthesized geopolymers.

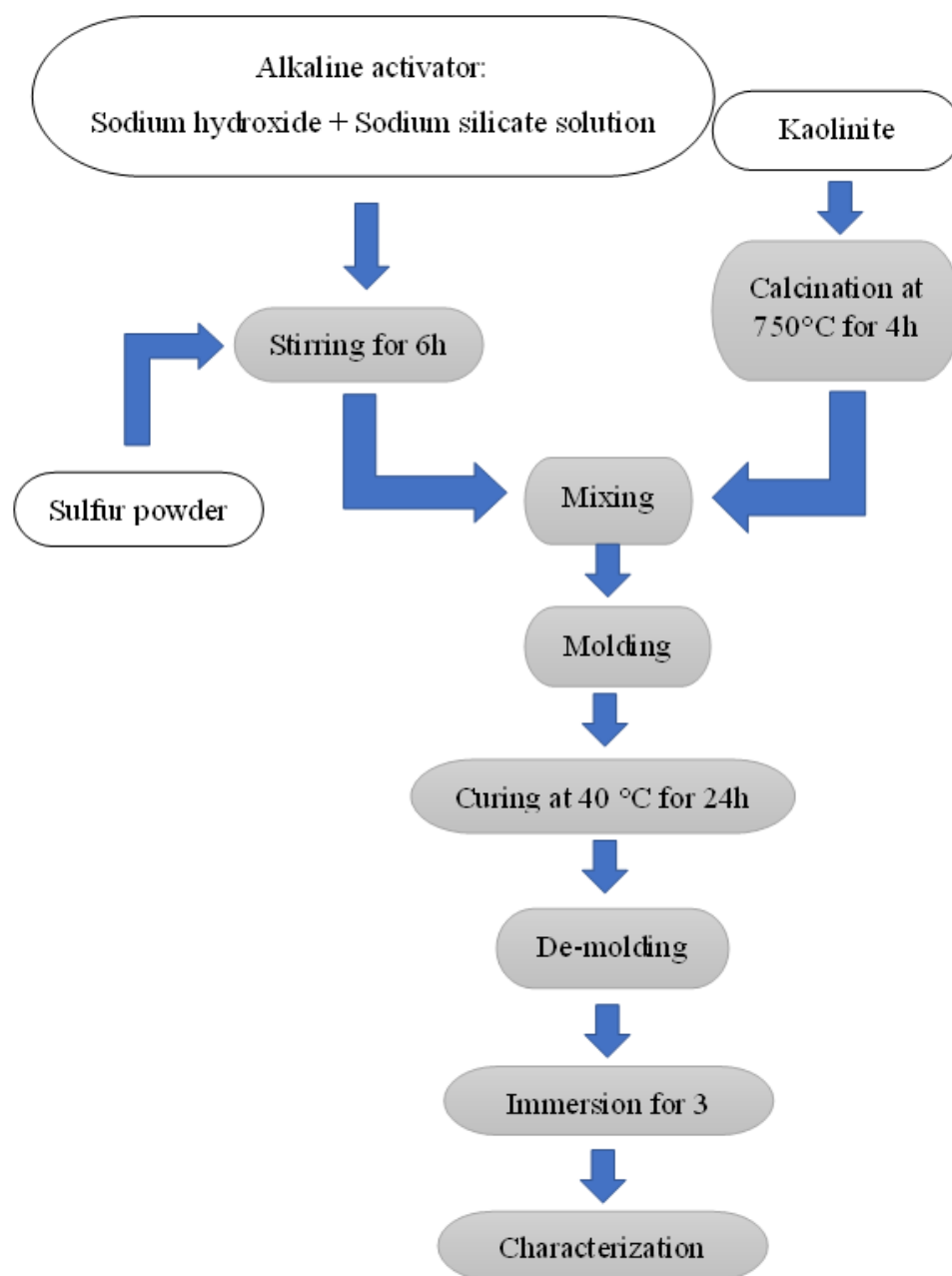| ID	Composition of Geopolymer Mixture (wt.%)				
	Metakaolin	Na_2SiO_3 Solution	NaOH	H_2O	S
GS0	100	100	25	48	0
GS2.5	100	100	25	48	2.5
GS5	100	100	25	48	5
GS10	100	100	25	48	10
GS15	100	100	25	48	15

Figure 1. Experimental procedure.

2.3. Characterization Techniques

To study the microstructure and the morphology of the produced geopolymers, the samples were first coated with platinum and then scanned using a scanning electron microscope (SEM) (QUANTA INSPECT F50, FEI Company, Eindhoven, The Netherlands). The thermal properties and the mass loss with heating were measured by heating the samples (~100 mg) using a thermogravimetric analyzer (TGA) (Netzsch, Germany, TG 209 F1 Libra). The temperature range was 50–800 °C with a 2 °C/min increment rate. This test was carried out in a helium environment. A qualitative mineralogical and phase analysis was carried out on the samples using a Shimadzu XRD diffractometer-6000 (Japan) with a cobalt tube and a 2-theta scanning range of 5−80° at a 2°/min scan rate. A Rietveld refinement of the produced materials was carried out using the software MATCH! (version 3.15, Crystal Impact, Bonn, Germany) with the fundamental parameter approach. FTIR spectra were obtained in the range of 4000–500 cm^{-1} using an FT-IR spectrometer (Perkin–Elmer system 2000, Waltham, MA, USA). The samples were subjected to compressive strength using a

universal testing machine (HD-B615-S, Dongguan, China). The machine-head speed was 1 mm/min. Three specimens of each series were subjected to this mechanical testing. The specimens' dimensions were height = 40 mm, width = 20 mm, and length = 20 mm. Inductively coupled plasma optical emission spectrometry (ICP-OES) was used to determine the cobalt content in the synthesized powders. The equipment used was a Thermo Scientific (iCAP 7000 series) (Thermo Fisher Scientific, Waltham, MA, USA).

3. Results and Discussion

3.1. Effect of Sulfur Loading on Compressive Strength of Geopolymers

The fraction of sulfur had a significant effect on the mechanical properties of the geopolymers, based on its function as a filler or a reactive component. However, it is not recommended to use sulfur as a filler because it is soluble and exposing it to water may result in a mechanical failure [24,25]. Therefore, based on this novel processing technique, the sulfur powder was completely dissolved in the alkaline solution before geopolymerization (Figure 1).

The variation in the compressive strength of the specimens (Table 1) is displayed in Figure 2. As can be seen, increasing the load of sulfur from 0 wt% to 5 wt%, compared with metakaolin, resulted in an increase in the compressive strength of the geopolymer from 22.5 MPa up to 29.9 MPa. However, when the content of sulfur was increased from 5 wt% up to 15 wt% in the geopolymers, a sharp decrease in the compressive strength, from 29.9 MPa to 15.7 MPa, was observed. This could be explained by the yellow color of the water after immersion, indicating that defects were caused in the geopolymer matrix through the solubility of the excess sulfur, resulting in the formation of voids and gaps. This type of defect, involving voids and gaps, could evolve into cracks during the compressive fracture processes of the material [26].
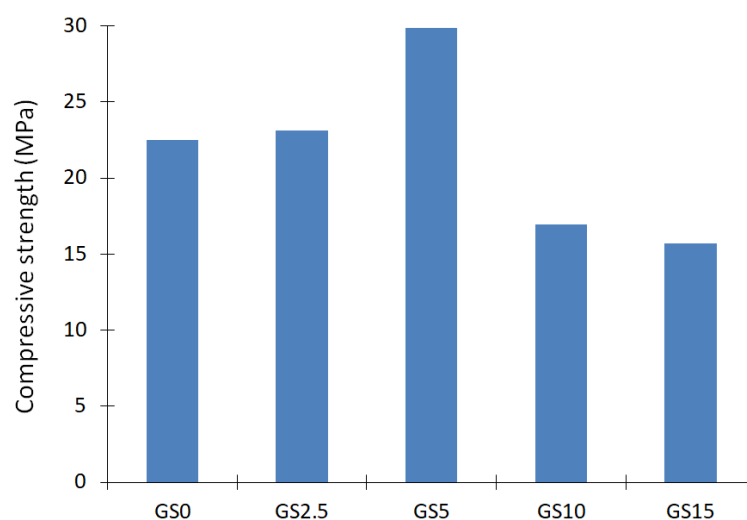

Figure 2. Compressive strength as a function of sulfur weight percentage (series GS0, GS2.5, GS5, GS10, and GS15 (Table 1)).

Compressive strength is a widely accepted measure to assess the performance of a given mixture. This characteristic is one of the major motivations to select the best material composition [26–28]. Therefore, the GS5 specimens were selected for further studies and analyses as the optimal composition.

3.2. The Role of Sulfur in Geopolymers

To determine the role of sulfur in geopolymers, an ICP analysis of the S/Al molar ratio in the resulting geopolymers was carried out after the geopolymers were washed with water to remove the soluble sulfur (Figure 3). The results of the end geopolymer products were compared with the S/Al ratio in the precursors.
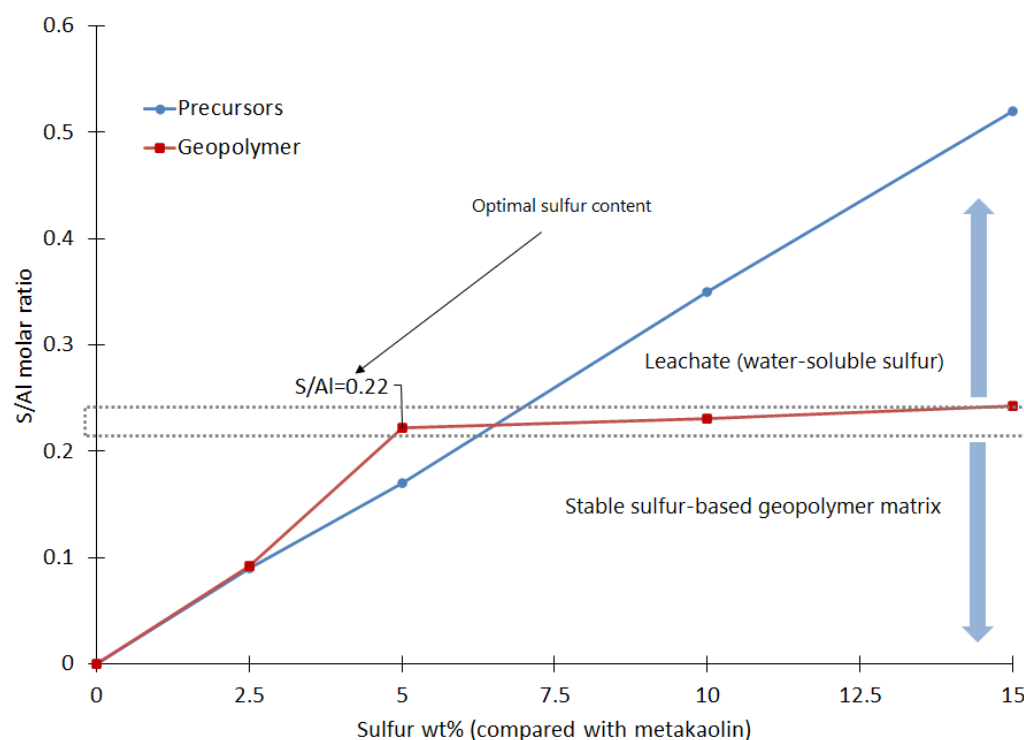
Figure 3. S/Al molar ratio of the precursors and the geopolymers (obtained using an ICP analysis).

It can be observed in Figure 3 that the S/Al molar ratio curves of the precursors and the geopolymers fit well below the S/Al molar ratio of 0.22, which is the molar ratio of GS5, and this confirms the chemical stabilization of sulfur in the geopolymer matrix. Within this range of S/Al molar ratios, the compressive strength of the geopolymers showed an increasing trend (Figure 2). For geopolymers with a S/Al molar ratio above 0.22, such as GS10 and GS15, the sulfur content of the geopolymers became almost constant, even when doubling, as in GS10, or tripling, as in GS15, the sulfur in the precursors. This confirms that all of the excess sulfur was dissolved and washed out as a leachate. Therefore, the defects in the geopolymer structure increased, and the mechanical properties thus deteriorated, as shown in Figure 2 for GS10 and GS15. These results confirm that the optimal S/Al molar ratio of the processes is around 0.22, which is the molar ratio of GS5, and the results are very consistent with the compression strength results described in the previous section.

3.3. Analysis of Microstructure and Phase Composition

Figure 4 shows the XRD scan analyses of the precursors, kaolinite and sulfur; the reference geopolymer (GS0); and the sulfur–geopolymer with an optimized composition based on the compressive strength factor (GS5) (Figure 2). The characteristic XRD peaks of the kaolinite and sulfur samples are easily observable in Figure 4A,B, respectively. The XRD pattern shown in Figure 4A illustrates that kaolinite also contains some minerals (TiO_2) with Miller indices of (011) and (004) and, in this case, 10.8% [14] (Table 3). The unit cell parameters and volume were slightly different from typical kaolinite, where the unit cell volume is 329.4 $\mathring{A}^3$ (Table 3), while the standard unit cell is 320.1 $\mathring{A}^3$ [27]. This change in the volume of the unit cell could be a result of the presence of impurities such as iron oxides, as reported in Table 1. Anatase is typically present in kaolin clay [11]. This metastable mineral represents one of the most common in titanium dioxide (TiO_2) with a tetragonal crystal structure [29].
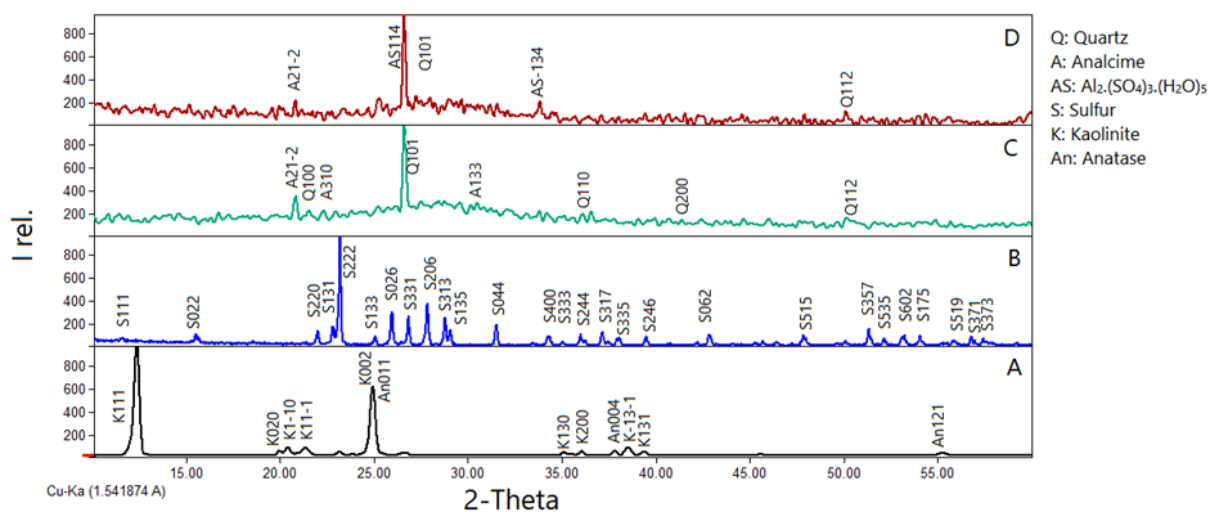
Figure 4. Qualitative XRD patterns for: (**A**) powdered kaolinite, K; (**B**) sulfur, S; (**C**) reference geopolymer, GS0; and (**D**) sulfur–geopolymer, GS5.

Table 3. Results of XRD analysis of the precursors (Rietveld refinement, MATCH! software).

Precursor	Phase	Phase %	Crystal Structure	a (Å)	b (Å)	c (Å)	V (Å^3)
Kaolinite	Kaolinite $Al_2Si_2O_5(OH)_4$	89.2	Triclinic *	5.15	8.94	7.40	329.4
	Anatase TiO_2	10.8	Tetragonal	3.78	-	9.51	135.9
Sulfur	S_8	100	orthorhombic	10.46	12.87	24.49	3296.8

* $\alpha = 91.7°$, $\beta = 104.7°$, $\gamma = 89.9°$.

The XRD pattern shows numerous peaks for sulfur at $2\theta = 23.13$, 25.90, and 27.78. Sulfur (S8) is characterized by an orthorhombic crystal structure with a unit cell specification of a = 10.48 Å, b = 12.87 Å, and c= 24.51 Å (Table 3).

As a result of the pre-treatment (calcination) and the subsequent chemical transformation (geopolymerization) of the precursors (Figure 4A), the XRD peaks corresponding to the kaolinite and anatase phases disappeared, leading to dissolution in the alkaline environment, as illustrated in Figure 4C for GS0. A hump observed in the XRD patterns between 20° and 40° (Figure 4C) confirms the formation of amorphous phases in the resultant geopolymer [9,30]. According to the Rietveld refinement analysis of the XRD data, the degree of GS0 crystallinity was 49.9%, and two crystalline phases were detected: triclinic analcime [29] and trigonal (hexagonal axes) quartz, with weight contents of 80.2% and 19.8, respectively (Table 4).

Introducing sulfur to the geopolymer's alkaline activator resulted in the diminishment of all of the peaks corresponding to this phase (Figure 4D). This is an indication of the incorporation of sulfur as a reactive component and a precursor in the geopolymer matrix instead of being a water-soluble filler. The degree of crystallinity of GS5 increased slightly, from 49.9% to 52.9%, with the addition of sulfur to the alkaline activator (Table 4). The XRD hump corresponding to the amorphous phase was detected between 22 °C and 35 °C. The crystalline phases of GS5 were similar to those of the metakaolin–polymer, GS0, but there was a new phase that was associated with sulfur, which was $Al_2H_{10}O_{17}S_3$ (Table 4). The percentage of this phase was 53.5% and it was characterized by its monoclinic crystal structure. Compared with GS0, the percentages of analcime and quartz decreased from 80.2% and 19.8% to 36.1% and 10.4%, respectively. There was also a reduction in the crystalline sizes of both analcime and quartz with the introduction of sulfur to the geopolymer matrix. These results confirm that sulfur reacts with aluminum from the metakaolin to form a new phase/s.

Table 4. Results of XRD analysis showing the crystallinity, phase composition, and crystal structure (Rietveld refinement, MATCH! software).

	Degree of Crystallinity	Crystalline Phase Composition	Phase %	Crystal System	Unit Cell Size (nm^3)	Crystalline Size (nm)
GS0	49.9%	$Al_{1.81} \cdot H4 \cdot Na_{1.71}O_{14}$ (analcime)	80.2	Triclinic	2.22835	152.7
		SiO_2 (quartz)	19.8	Hexagonal	0.113526	179.5
GS5	52.9%	$Al_{1.81} \cdot H4 \cdot Na_{1.71}O_{14}$ (analcime)	36.1	Triclinic	2.22835	93.5
		SiO_2 (quartz)	10.4	Hexagonal	0.113526	68.7
		$Al_2H_{10}O_{17}S_3$	53.5	Monoclinic	1.226255	75.9

The metakaolin layers, as the main precursors and the sources of Al ions for the geopolymer, were reported as the SEM, as shown in Figure 5B (point 2). These layers were distorted due to the calcination of kaolinite at 750 °C. The SEM analysis, shown in Figure 5C, indicates that the microstructure of GS0 is composed of binder material (geopolymer matrix) (point 3) and partially dissolved metakaolin layers (point 4). This SEM image also shows that, as a result of geopolymerization and the setting reactions, the gaps between partially dissolved metakaolinite layers were filled with formed binding material (sodium aluminosilicate matrix) [30].
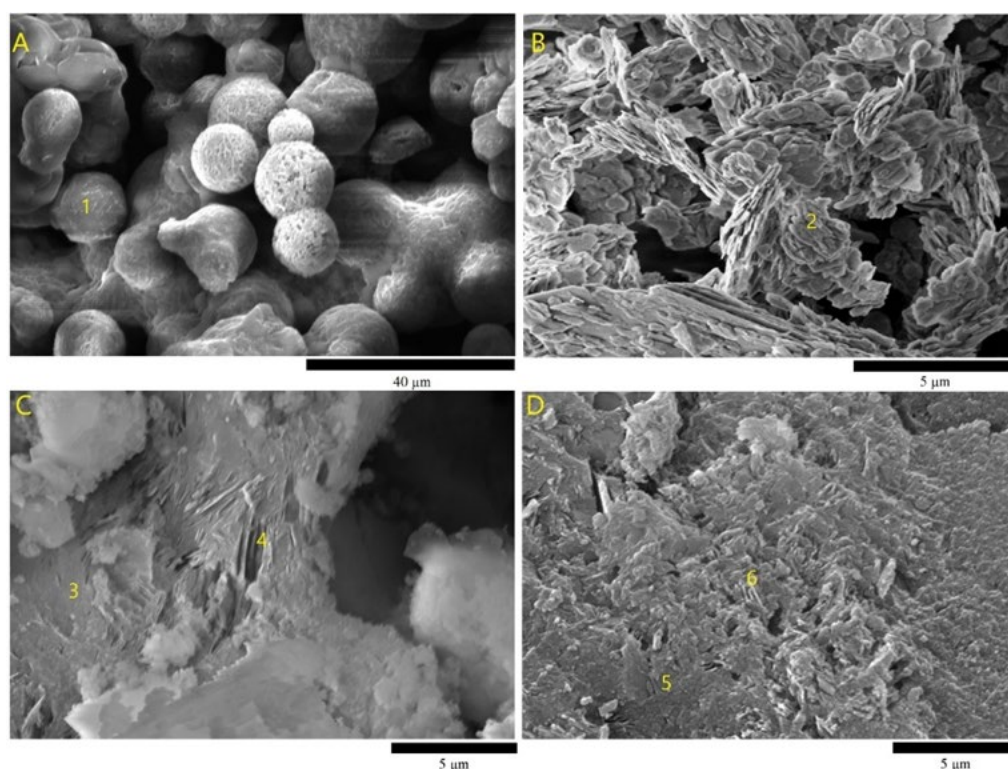

Figure 5. SEM images of: (**A**) sulfur; (**B**) metakaolin; (**C**) GS0 geopolymer; and (**D**) GS5 geopolymer; (1) sulfur, (2) metakaolin layers, (3, 5) geopolymer matrix, and (4, 6) voids resulting from the dissolution of metakaolin.

The produced geopolymers exhibited a structure of a nano-porous network formed by aluminosilicate particles [31]. The size of the aluminosilicate particles (~160 nm) (Table 4), which were encapsulated in the geopolymer matrix, determined the nano-pore pattern observed in the microstructure (Figure 6A). The formation of a uniform pore structure and a homogeneous pore network of aluminosilicate particles can be observed in Figure 6A. This finding is in agreement with the results reported by Alshaaer et al. [32], who produced partially amorphous sodium aluminosilicates after the activation of metakaolin with alkali

activators. Sulfur microspheres of ~10 μm, were confirmed using a scanning electron microscope (SEM) (Figure 5A, point 1). The addition of sulfur showed that the microstructure of GS5 is characterized by the following main phases: the geopolymer matrix (Figure 5D, point 5) and the voids (Figure 5D, point 6) associated with the dissolution of metakaolin during the geopolymerization process. When the SEM magnification was increased, as shown in Figure 6, the emergence of a more compacted, i.e., less nonporous, microstructure was observed (Figure 5B), compared with GS0 (Figure 6A). This may have an important impact on the physical and chemical properties of the end geopolymer products.

Figure 6. SEM images with a high magnification of: (**A**) metakaolin-based geopolymer, GS0; and (**B**) sulfur-based geopolymer, GS5.

3.4. FTIR Spectra of Geopolymers (GS0 and GS5)

The FTIR spectra of GS0 and GS5 are shown in Figure 7. In the spectrum of GS0, the peaks at 594 cm^{-1}, 660 cm^{-1}, and 984 cm^{-1} are attributed to the Si-O-Al, Si-O-Al, and Si–O-Si bonds, respectively [33]. The appearance of these three peaks was also observed in the results for GS5, and they are indicative of the limited change in the bonding by adding sulfur to the alkaline activator (GS5). The absorption bands at about 594 cm^{-1} and 660 cm^{-1} on both the GS0 and GS5 spectra are, respectively, attributed to the asymmetric and symmetric vibrations of the Si-O-Al and Si-O-Si bonds that provide the cohesion between the AlO_4 and SiO_4 tetrahedrons in the geopolymer structure [34].

In the spectrum of geopolymer GS0 in Figure 7, the band at 1370 cm^{-1} can be assigned to O–C–O, which was also observed for GS5. This band is related to the presence of sodium carbonate via the reaction of alkali metal hydroxide with atmospheric CO_2 [35,36]. These peaks are clearly presented in the spectrum of GS5, which suggests the existence of a geopolymer. The absorption broadbands at 1650 cm^{-1} and 3340 cm^{-1} are the stretching and bending vibration frequencies of the OH groups associated with water [34]. The strong and broad absorption band centered at 613 cm^{-1} in the GS5 spectrum probably also resulted from the combined absorptions of SO_4^{-2} and the Si–O–Al stretching vibrations. The strong band centered at 998 cm^{-1} could be due to the combination of sulfate absorptions and the Si–O–Al band [35].

The FTIR spectra confirmed the geopolymer structure of both GS0 and GS5 [36]. There is a clear similarity between the FTIR spectra of geopolymers GS0 and GS5. This similarity is probably due to the small proportion of sulfur, comprising about 1.8% of the total mix, that was added to the precursors of GS5. Another possibility is the apparent overlap in the sulfate spectra with silica and aluminum bonds [37].
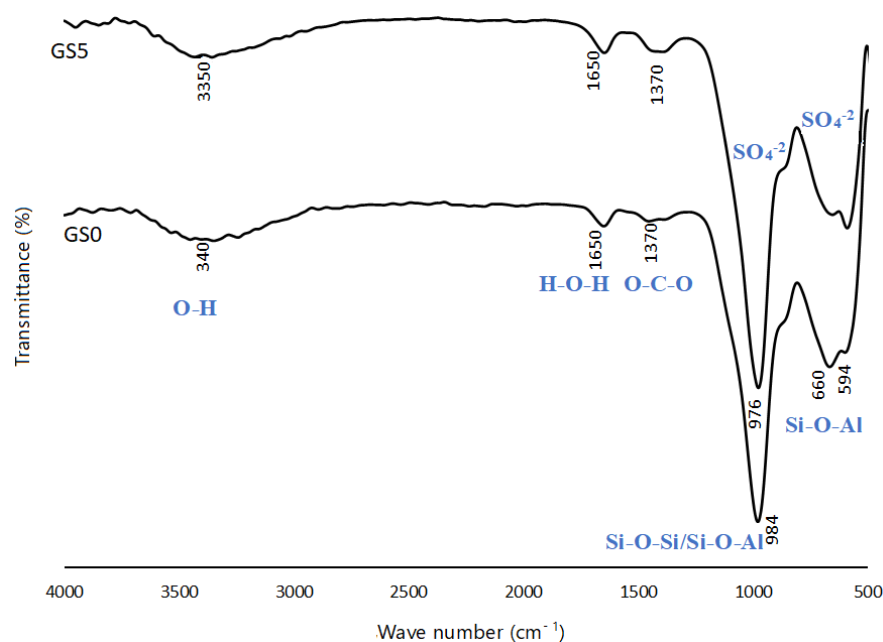
Figure 7. FTIR spectra of geopolymers (GS0 and GS5).

3.5. Thermogravimetric Analysis (TGA)

The thermal decomposition process of GS0 and GS5 in air was investigated using TG tests, and the corresponding results are given in Figure 8. The total weight loss as a result of heating the GS0 up to 800 °C was around 15.9% (Figure 8A). This cumulative mass loss increased to 18.4% after the addition of sulfur (GS5). The overall increment in mass loss was due to the presence of more structural water, attributed to the new phases, i.e., $Al_2 \cdot H_{10} \cdot O_{17} \cdot S_3$ (Table 4). The evaporation of sulfur at relatively low temperatures of less than 300 °C [38] may be one of the causes of this increase in weight loss, but it is certainly not the main reason, as the total sulfur constituents, at 1.8%wt, were less than the difference in weight loss, which was 2.5%.

The derivative of the TGA curve reveals that thermal events occur in two main temperatures ranges, 50–250 °C and 500–700 °C, as shown in Figure 8B. In the first range (25–200 °C), the decrease in weight is associated with the release of fine-pore moisture. In the second range (500–700 °C), the decrease in weight can be attributed to the release of zeolitic water from the nano-porous network [32].

Previous studies [38] have concluded that the sulfur begins to evaporate at 250 °C and disappears completely at about 350 °C. This rapid weight loss of sulfur is attributable to the collapse of S–S bonds. However, it can be observed in Figure 8B that there is no increase in the percentage of weight loss for GS5 compared to GS0, so sulfur as an element can be considered to have no presence in the structure of GS0. Thus, sulfur is associated with essential elements in geopolymers such as aluminum, as confirmed by the formation of $Al_2 \cdot H_{10} \cdot O_{17} \cdot S_3$ (Table 4).

The presence of elemental sulfur in the microstructure of geopolymers leads to its dissolution in water, which turns yellow, as shown by GS10 and GS15 (Table 1). Thus, elemental sulfur leaves voids, resulting in a decrease in its mechanical performance (Figure 1). An increase in weight loss in the second range, 500–700 °C, is likely due to the release of $Al_2 \cdot H_{10} \cdot O_{17} \cdot S_3$ structural water [39].
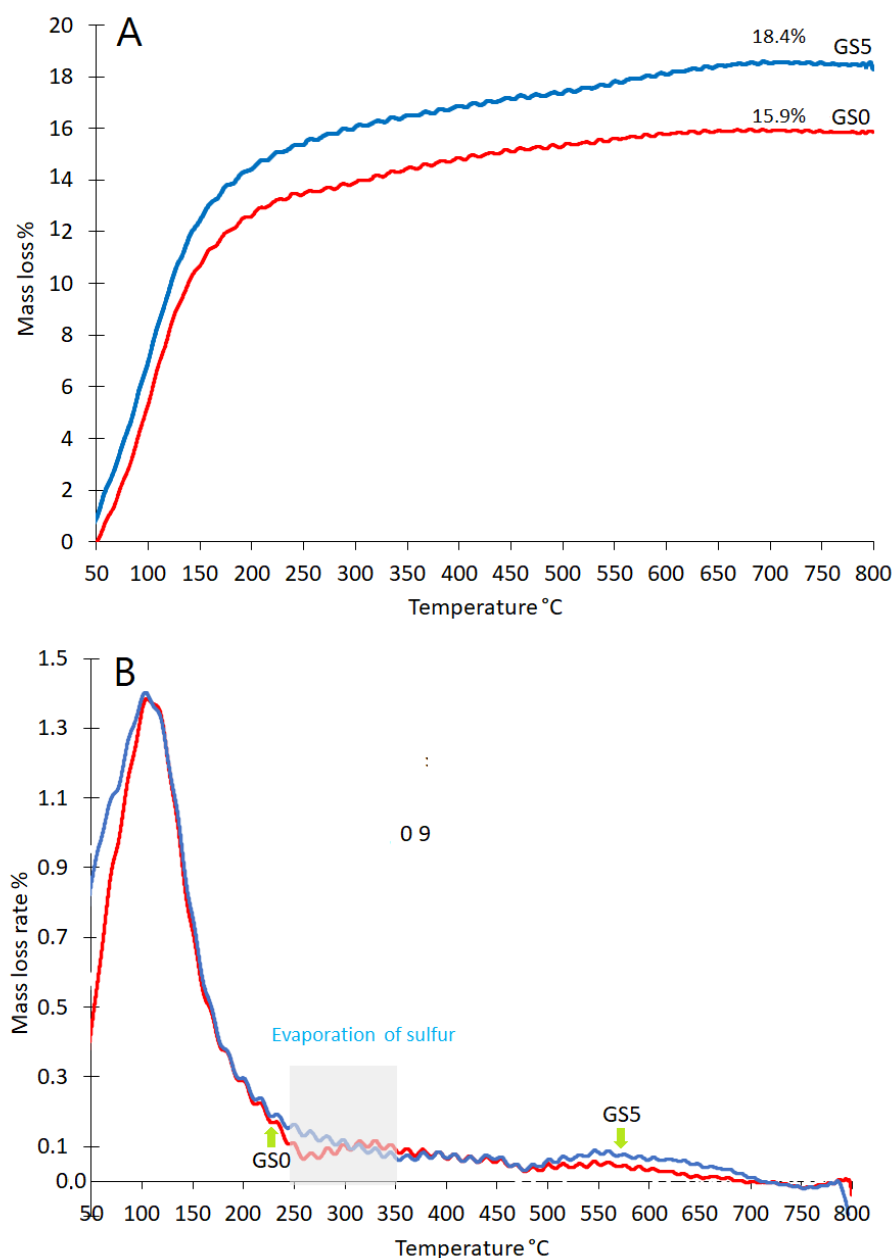
Figure 8. TGA of geopolymers GS0 and GS1: (**A**) cumulative TGA; and (**B**) differential TGA.
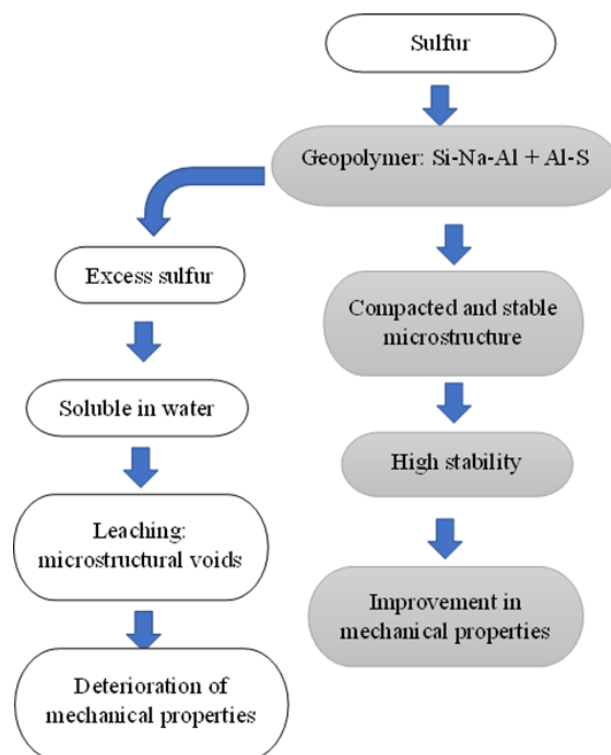
3.6. Influence of S/Al Molar Ratio on Geopolymer Properties

The above-mentioned results show that sulfur can have both positive and negative effects on the mechanical properties and stability of geopolymers. Sulfur was first dissolved in the alkaline solution, and then metakaolin was added. Sulfur reacted with Al to form new phases, such as $Al_2 \cdot H_{10} \cdot O_{17} \cdot S_3$. The resultant microcrystalline structure was composed of compacted nano-crystalline/amorphous phases. Sulfur decreased the crystalline sizes of both quartz and analcime. As a result of these microstructural changes, an improvement in the mechanical properties was observed, where the compressive strength increased by ~32% (Figure 2).

Increasing the S/Al molar ratio from 0.17 up to 0.52 (Table 5) led to the precipitation of excess sulfur, or unreacted sulfur, in the matrix. The excess sulfur dissolved when the material was exposed to water, and a leaching process took place. As a result of this sulfur leaching, defects and voids were left in the microstructure; thus, its mechanical properties deteriorated (Figure 9).

Table 5. S/Al molar ratio of the geopolymers (ICP analysis).

ID	S/Al Molar Ratio	
	Precursors	Geopolymers
GS0	0.00	0.00
GS2.5	0.09	0.09
GS5	0.17	0.22
GS10	0.35	0.23
GS15	0.52	0.24

Figure 9. Influence of sulfur on geopolymer properties.

4. Conclusions

This study had two major goals. The first goal was to introduce a novel synthesis method for sulfur-based geopolymers. This goal was achieved by integrating sulfur into the geopolymer matrix chemically and preventing it from washing out as a leachate. The second goal was to determine the optimal content of sulfur to produce geopolymers with good mechanical properties. It was observed that the optimal S/Al molar ratio of the precursors is around 0.17. Sulfur reacted with Al to form new phases, such as $Al_2 \cdot H_{10} \cdot O_{17} \cdot S_3$. The resultant microcrystalline structure was composed of compacted nano-crystalline/amorphous phases. Sulfur decreased the crystalline sizes of both quartz and analcime. As a result of these microstructural changes, an improvement in the mechanical properties was observed, where the compressive strength increased by ~32%. Increasing the S/Al molar ratio from 0.17 up to 0.5 led to the precipitation of excess sulfur, or unreacted sulfur, in the matrix. The excess sulfur dissolved when the material was exposed to water, and a leaching process took place. As a result of this sulfur leaching, defects and voids were left in the microstructure; thus, its mechanical properties deteriorated. The role of sulfur in geopolymers, whether as a precursor or a water-soluble filler, was explained by comparing the S/Al molar ratio of the precursors and the geopolymers using an ICP analysis. Different tests have confirmed that sulfur interacts with aluminum ions from the metakaolin and is incorporated into the microstructure of geopolymers. The crystalline phases of the resulting geopolymers clearly change after the addition of sulfur. The SEM

analysis showed that the microstructure of the geopolymers became denser and more compact after the addition of sulfur. The FTIR spectrum analysis did not show significant differences after the addition of sulfur, and this was explained by interference bands of sulfate as well as silica and aluminum bands. The TG analysis confirmed that there was no unreacted sulfur in the microstructure of the geopolymers, although it was added to the precursors and dissolved in the alkaline solution. From this study, we concluded that sulfur can be used initially to improve the properties of geopolymers and facilitate the emergence of new phases and microstructural characteristics. Adding sulfur to the alkaline solution in higher levels leads to the precipitation of elemental sulfur in the geopolymer microstructure; thus, the sulfur becomes soluble in water, resulting in the deterioration of the geopolymer's mechanical performance.

References

1. Ober, J. *Materials Flow of Sulfur*; U.S. Geological Survey: Reston, VA, USA, 2002.
2. Fediuk, R.; Mugahed, A.Y.; Mosaberpanah, M.; Danish, A.; El-Zeadani, M.; Klyuev, S.; Vatin, N. A Critical Review on the Properties and Applications of Sulfur-Based Concrete. *Materials* **2020**, *13*, 4712. [CrossRef]
3. Fediuk, R.S.; Yevdokimova, Y.G.; Smoliakov, A.K.; Stoyushko, N.Y.; Lesovik, V.S. Use of geonics scientific positions for designing of building composites for protective (fortification) structures. *IOP Conf. Ser. Mater. Sci. Eng.* **2017**, *221*, 012011. [CrossRef]
4. Wagenfeld, J.-G.; Al-Ali, K.; Almheiri, S.; Slavens, A.F.; Calvet, N. Sustainable applications utilizing sulfur, a by-product from oil and gas industry: A state-of-the-art review. *Waste Manag.* **2019**, *95*, 78–89. [CrossRef]
5. Stern, D.I. Reversal of the trend in global anthropogenic sulfur emissions. *Glob. Environ. Chang.* **2006**, *16*, 207–220. [CrossRef]
6. Eliseev, A.V. Climate change mitigation via sulfate injection to the stratosphere: Impact on the global carbon cycle and terrestrial biosphere. *Atmos. Ocean. Opt.* **2012**, *25*, 405–413. [CrossRef]
7. Komnitsas, K.; Zaharaki, D.; Perdikatsis, V. Effect of synthesis parameters on the compressive strength of low-calcium ferronickel slag inorganic polymers. *J. Hazard. Mater.* **2009**, *161*, 760–768. [CrossRef]
8. Komnitsas, K.; Zaharaki, D.; Perdikatsis, V. Geopolymerisation of low calcium ferronickel slags. *J. Mater. Sci.* **2007**, *42*, 3073–3082. [CrossRef]
9. Yu, G.; Jia, Y. Microstructure and Mechanical Properties of Fly Ash-Based Geopolymer Cementitious Composites. *Minerals* **2022**, *12*, 853. [CrossRef]
10. Lo, K.-W.; Lin, W.-T.; Lin, Y.-W.; Cheng, T.-W.; Lin, K.-L. Synthesis Metakaolin-Based Geopolymer Incorporated with SiC Sludge Using Design of Experiment Method. *Polymers* **2022**, *14*, 3395. [CrossRef]
11. Khatib, K.; Lahmyed, L.; El Azhari, M. Synthesis, Characterization, and Application of Geopolymer/TiO2 Nanoparticles Composite for Efficient Removal of Cu(II) and Cd(II) Ions from Aqueous Media. *Minerals* **2022**, *12*, 1445. [CrossRef]
12. Komnitsas, K.; Zaharaki, D.; Vlachou, A.; Bartzas, G.; Galetakis, M. Effect of synthesis parameters on the quality of construction and demolition wastes (CDW) geopolymers. *Adv. Powder Technol.* **2015**, *26*, 368–376. [CrossRef]
13. Ahmed, D.A.; El-Apasery, M.A.; Aly, A.A.; Ragai, S.M. Green Synthesis of the Effectively Environmentally Safe Metakaolin-Based Geopolymer for the Removal of Hazardous Industrial Wastes Using Two Different Methods. *Polymers* **2023**, *15*, 2865. [CrossRef] [PubMed]

14. Alshaaer, M.; Abu Mallouh, S.A.; Al-Kafawein, J.; Al-Faiyz, Y.; Fahmy, T.; Kallel, A.; Rocha, F. Fabrication, microstructural and mechanical characterization of Luffa Cylindrical Fibre—Reinforced geopolymer composite. *Appl. Clay Sci.* **2017**, *143*, 125–133. [CrossRef]

15. El Alouani, M.; Saufi, H.; Moutaoukil, G.; Alehyen, S.; Nematollahi, B.; Belmaghraoui, W.; Taibi, M. Application of geopolymers for treatment of water contaminated with organic and inorganic pollutants: State-of-the-art review. *J. Environ. Chem. Eng.* **2021**, *9*, 105095. [CrossRef]

16. Geissdoerfer, M.; Savaget, P.; Bocken, N.; Hultink, E.J. The Circular Economy—A new sustainability paradigm? *J. Clean. Prod.* **2017**, *143*, 757–768. [CrossRef]

17. El-Eswed, B.; Yousef, A.M.; Hamadneh, I.; Al-Gharabli, S.; Khalili, F. Stabilization/solidification of heavy metals in kaolin/zeolite based geopolymers. *Int. J. Miner. Process.* **2015**, *137*, 34–42. [CrossRef]

18. Kinnunen, P.; Ismailov, A.; Solismaa, S.; Sreenivasan, H.; Räisänen, M.-L.; Levänen, E.; Illikainen, M. Recycling mine tailings in chemically bonded ceramics—A review. *J. Clean. Prod.* **2018**, *174*, 634–649. [CrossRef]

19. Tian, Q.; Bai, Y.; Pan, Y.; Chen, C.; Yao, S.; Sasaki, K.; Zhang, H. Application of Geopolymer in Stabilization/Solidification of Hazardous Pollutants: A Review. *Molecules* **2022**, *27*, 4570. [CrossRef]

20. Shi, C.; Fernández-Jiménez, A. Stabilization/solidification of hazardous and radioactive waste with alkali-activated cements. *J. Hazard. Mater.* **2006**, *137*, 1656–1663. [CrossRef]

21. Luukkonen, T.; Runtti, H.; Niskanen, M.; Tolonen, E.-T.; Sarkkinen, M.; Kemppainen, K.; Rämö, J.; Lassi, U. Simultaneous removal of Ni(II), As(III), and Sb(III) from spiked mine effluent with metakaolin and blast-furnace-slag geopolymers. *J. Environ. Manag.* **2016**, *166*, 579–588. [CrossRef]

22. Keane, P.F.; Jacob, R.; Belusko, M.; Bruno, F. Self-Healing Glass/Metakaolin-Based Geopolymer Composite Exposed to Molten Sodium Chloride and Potassium Chloride. *Appl. Sci.* **2023**, *13*, 2615. [CrossRef]

23. Alshaaer, M. Synthesis, Characterization, and Recyclability of a Functional Jute-Based Geopolymer Composite. *Front. Built Environ.* **2021**, *7*, 631307. [CrossRef]

24. Maldonado-Zagal, S.B.; Boden, P. Hydrolysis of Elemental Sulphur in Water and its Effect on the Corrosion of Mild Steel. *Br. Corros. J.* **1982**, *17*, 116–120. [CrossRef]

25. Ferreira, A.G.M.; Lobo, L. The low-pressure phase diagram of sulfur. *J. Chem. Thermodyn.* **2011**, *43*, 95–104. [CrossRef]

26. Ashby, M.F.; Sammis, C.G. The Damage Mechanics of Brittle Solids in Compression. *Pure Appl. Geophys.* **1990**, *133*, 489–521. [CrossRef]

27. Zhu, C.; He, M.-C.; Jiang, B.; Qin, X.-Z.; Yin, Q.; Zhou, Y. Numerical investigation on the fatigue failure characteristics of water-bearing sandstone under cyclic loading. *J. Mt. Sci.* **2021**, *18*, 3348–3365. [CrossRef]

28. Yin, Q.; Wu, J.; Zhu, C.; He, M.; Meng, Q.; Jing, H. Shear mechanical responses of sandstone exposed to high temperature under constant normal stiffness boundary conditions. *Geomech. Geophys. Geo-Energy Geo-Resour.* **2021**, *7*, 35. [CrossRef]

29. Nesse, W.D. *Introduction to Mineralogy*; Oxford University Press: New York, NY, USA, 2000; pp. 254–255.

30. Bukhary, A.; Azam, S. A Review of Physicochemical Stabilization for Improved Engineering Properties of Clays. *Geotechnics* **2023**, *3*, 744–759. [CrossRef]

31. Kupwade-Patil, K.; Allouche, E. Impact of alkali silica reaction on fly ash-based geopolymer concrete. *J. Mater. Civ. Eng.* **2011**, *25*, 131–139. [CrossRef]

32. Alshaaer, M.; Al-Fayez, Y.J.; Fahmy, T.; Hamaideh, A. Synthesis of geopolymer cement using natural resources for green construction materials. In *Recent Advances in Earth Sciences, Environment and Development, Proceedings of the 8th International Conference on Engineering Mechanics, Structures, Engineering Geology (EMESEG'15), Konya, Turkey, 20–22 May 2015*; Bulucea, A., Koçak, K., Ntalianis, K., Eds.; WSEAS Press: Athens, Greece, 2015.

33. Huang, Y.; Gong, L.; Pan, Y.; Li, C.; Zhou, T.; Cheng, X. Facile construction of the aerogel/geopolymer composite with ultra-low thermal conductivity and high mechanical performance. *RSC Adv.* **2018**, *8*, 2350–2356. [CrossRef]

34. Nmiri, A.; Yazoghli, O.; Duc, M.; Hamdi, N.; Srasra, E. Temperature effect on mechanical and physical proprieties of Na or K alkaline silicate activated metakaolin-based geopolymers. *Ital. J. Eng. Geol. Environ.* **2016**, *1*, 5–15.

35. Chindaprasirt, P.; Jaturapitakkul, C.; Chalee, W.; Rattanasak, U. Comparative study on the characteristics of fly ash and bottom ash geopolymers. *Waste Manag.* **2009**, *29*, 539–543. [CrossRef] [PubMed]

36. Kumar, S.; Kristály, F.; Mucsi, G. Geopolymerisation behaviour of size fractioned fly ash. *Adv. Powder Technol.* **2014**, *26*, 24–30. [CrossRef]

37. Serna, C.J.; White, J.L.; Hem, S.L. Anion-Aluminum Hydroxide Interactions. *Soil Sci. Soc. Am. J.* **1977**, *42*, 1009–1013. [CrossRef]

38. Zhang, S. Understanding of Sulfurized Polyacrylonitrile for Superior Performance Lithium/Sulfur Battery. *Energies* **2014**, *7*, 4588–4600. [CrossRef]

39. Van Essen, M.; Gores, J.; Bleijendaal, L.; Zondag, H.; Schuitema, R.; Helden, W. Characterization of salt hydrates for compact seasonal thermochemical storage. In Proceedings of the 11th International Conference on Thermal Energy Storage, Stockholm, Sweden, 14–17 June 2009.